Numerical Modelling of a Sinusoidal Grating-based Surface Plasmon Coupled Emission Biosensor

V. Sukhotskiy[†], N.C. Cady[‡], E. Chou[‡], I.V.A.K Reddy[†], E.P. Furlani[†‖]
[†]Department of Electrical Engineering, University at Buffalo SUNY
[‡] Department of Nanobioscience, SUNY Polytechnic Institute ALBANY
[‖]Department of Chemical and Biological Engineering, University at Buffalo SUNY

ABSTRACT

In this paper, we present a full-wave computational model to study the optical behavior of a versatile sinusoidal grating-based surface plasmon–coupled emission (SPCE) biosensor. Surface plasmons are coherent oscillations of conduction electrons on a metal surface excited by incident light at the metal-dielctric interface. The sensitivity of the surface plasmon resonance (SPR) to a change in refractive index at the interface has led to the development ultra-sensitive SPR sensing systems, which typically use prisms to couple light into a single SP mode on flat, continuous metal film (typically gold). In this work, we present a rigorous full-wave analysis of a sensor composed of a SiO_2 substrate coated with a titanium (Ti) adhesion layer and a 45 nm gold layer. Our predictions are in agreement with the recorded data. We demonstrate the model and its potential for the rational design of new sensor systems

Keywords: Surface plasmon resonance, SPR grating, biosensing, sinusoidal grating

1 INTRODUCTION

Since the discovery of surface plasmon resonance by Otto [1] and Kretschmann [2] there has been intense interest in, and growing appplications of, SPR-based biosening technology. SPR-based biosensing has several advantages over more convential sensing methods in terms of reliability, sensitivity and throughput [3]. In SPR, polarized light is used to excite plasmons on dielectric-metal interface. These plasmons are extremely sensitive to any change in refractive index at this interface. This provides a key mechanism for biosensing [4]. Conventional SPR biosensing techniques use the Kretschmann configuration, which is prism based detection technique. A relatively large detection spot [4] and the need for bulky prisms make this approach awkward for compact and miniatured biosensing platforms. Grating-coupled surface plasmon resonance (GCSPR) [5,6] has gained popularity in the recent years as it can easily overcome the limitations posed by prism-coupling. GCSPR uses a diffraction grating to excite plasmons. Unlike prism-coupling that uses higher refractive index material (dielectric) for momentum matching, diffraction gratings use Bragg scattering [7]. In this phenomena, the wavevector of incident photon is added to integer multiples of the grating-generated field vector. However, surface plasmons are only possible if the photons are incident at a specific angle. Other crucial parameters that affect the sensitivity are the shape, depth and thickness of the grating grooves [7,8]. In this paper, we present a computational model for predicting the optical behavior of the grating and use the model to generate optimal parameters for surface plasmon excitation. To complement our results, we also present an experimental validation with a fabricated GCSPR chip and show its potential for disease diagnosis.

2 THEORY

In order to excite surface plasmons, we need to match the momentum of incident photons with the planar surface plasmon wavevector [7,9]. The surface plasmon wave (k_{sp}) is given by [5,7]

$$k_{sp} = k_0 \sqrt{\frac{\varepsilon_d \varepsilon_m}{\varepsilon_d + \varepsilon_m}} ,$$

where k_0 is the freespace waveevector of light, ε_d and ε_m are the relative permittivities of dielectric and metal, respectively. As this momentum can not be achieved on a smooth metal surface, we use diffraction gratings. The grating produces series of diffracted waves when a plane wave is incident on it. In this situtation, multiple grating vectors superimpose with photon incident wave vector, which results in the matching of momentum [7]. The equation governing this is give by:

$$k_0 \sqrt{\varepsilon_d} \sin\theta_R + m\frac{2\Pi}{\Lambda} = \pm k_0 \sqrt{\frac{\varepsilon_d \varepsilon_m}{\varepsilon_d + \varepsilon_m}}$$

where θ_R is the resonance angle, m is an integer and it represents diffraction orders, Λ is the grating period, sign ' $\pm$ ' correspond to positive and negative diffraction orders.

3 COMPUTATIONAL MODEL

We used the finite element (FEA)-based COMSOL program 5.3a (www.comsol.com) for the computational model. Specifically, the COMSOL Electromagnetics RF module was used for this work. A full-wave time-harmonic analysis is used wherein the field satsifies:

$$\nabla \times \left(\mu_r^{-1} \nabla \times E \right) - k_0^2 \left(\varepsilon_r - j \frac{\sigma}{\omega \varepsilon_0} \right) E = 0$$

where ε_r, μ_r and σ are relative permittvity, permeability and conductivity of the media. For gold or silver, we use a dispersive Drude-like dielctric function [10,11]. As a first step, we simulate different grating profiles, i.e. sinusoidal, rectangular and trapezoidal. This is to validate the use of a sinusoidal grating. We chose a period depending on the experimental limitations in fabrication. However, the grating thickness of the plasmonic layer is varied to study its impact on the SPR excitation. Based on this analysis, the final sensor is composed of a SiO_2 substrate coated with Ti adhesion layer and a 45 nm Au layer, as shown in Fig. 1(d). Since the grating is periodic, we simulated a part of grating with periodic boundary conditions on the lateral walls. A periodic port is used for the wave excitation. A TM polarized wave is used for exciting surface plasmons.

4 RESULTS AND DISCUSSION

Grating Profile: The profile of a grating plays a critical role in its sensing performance. Currently, different types of gratings with rectangular [12], hexagonal [8] and trapezoidal [7] profiles are being used. However, the practical realization of gratings with sharp edge profiles are difficult to fabricate. On the other hand, sinusoidal gratings are relatively easier to fabricate due to their smoothly varying egdes and can servee as an approximation to rectangular/square gratings [12]. Here, we investigate various grating profiles, trapezoidal and triangular, and compare their optical response with that of a of sinusoidal profile. As shown in Fig.1 (a), the nonsinusoidal gratings generate either a weak reflectivity or a broad resonance peak. This is not a desirable output for sesning applications. However, in contrast, sinusoidal gratings generate a sharp resonance peak with a very good reflectvity (as shown in Fig.2(a)).

Grating Period: The grating period Λ is varied from 450 nm to 600 nm in 50 nm increments (Fig.2(b)). We observe a sharp resonance when Λ is 450 and 500 nm. However as Λ increases, the resonance broadens.

Grating Depth: We varied the depth of grating grooves *h* from 25 nm to 100 nm in 25 nm increments (Fig.2(c)). As *h* increases, the peak becomes sharper with good reflectivity and then gradually suffers a reduction in reflectivity. The optimal parameter for *h* is near 50 nm. A 45 nm gold layer is used for the final sesnor.

Grating Material: Although various metals like gold, silver, aluminum etc. can excite plasmons [3], gold and silver are commonly used due to their sesnitivity and biocompatability [13]. We investigate these two metals on a sinusoidal grating with the following parameters: Λ = 500 nm, *h* = 45nm and incident waevlength λ= 633 nm. We observe that both silver and gold show similar resonance,

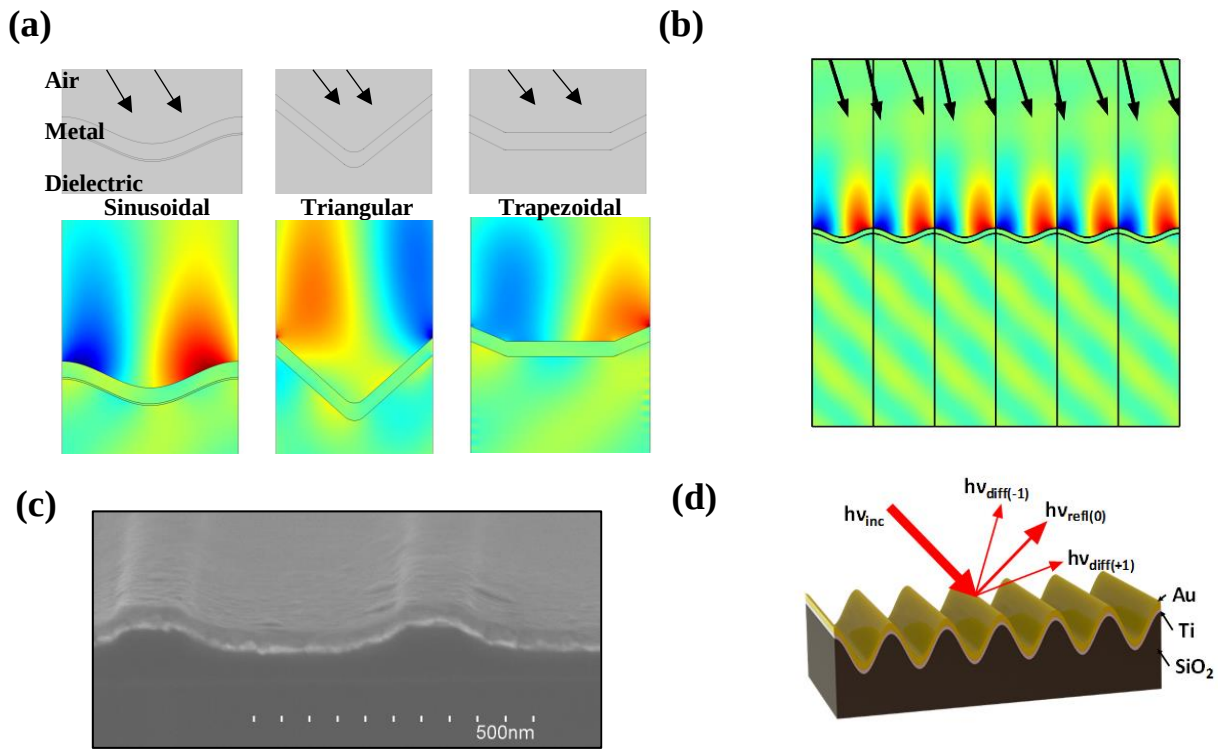

Figure 1: (**a**) varying the geometries of gratings and their corresponding resonance – sinusoidal, triangular and trapezoidal, (**b**) Surface plasmon reonnace observed on the surface of an array of simusoidal grating, (**c**) SEM image of sinusoidal grating fabricated, (**d**) diffraction gratings depicted with sinusoidal gratings

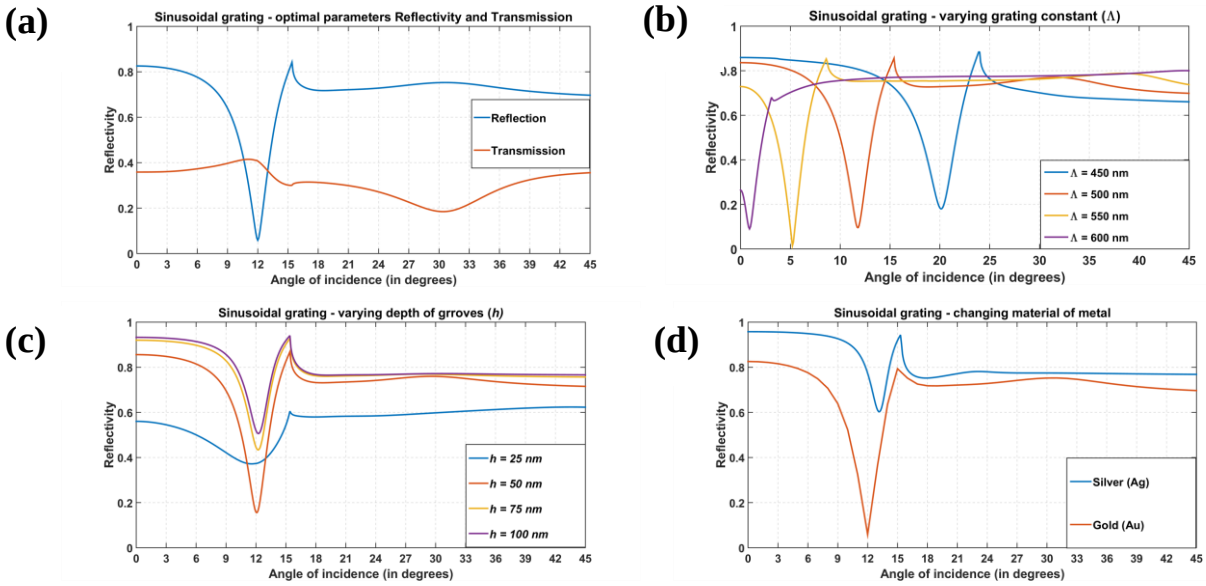

Figure 2: plot demonstrating (a) reflectivity and transmission of a sinusoidal grating with optimal parameters (b)effect of varying depth of grooves (c) effect of varying grating constant (d) varying material – gold and silver coated gratings.

but gold seems to be more promising wih this particular mix of grating parameters. In summary, we choose a sinusoidal gold grating with Λ 500 nm and *h* near 50 nm to obtain optimal performance.

5 EXPERIMENTAL VERIFICATION

We fabricated GCSPR microchips with the parameters defined above. The sensors were fabricated on 300 mm diameter silicon wafers coated with a 50 nm layer of tetraethyl orthosilicate (TEOS) and a layer of photoresist. Immersion photolithography (193 nm wavelength) was used to pattern the photoresist layer with a sub-micrometer optical SPR grating pattern with dimensions of 250 nm lines on a 500 nm pitch. Following the development of the photoresist, reactive ion etching was used to etch the TEOS layer in the exposed regions, resulting in a three-dimensional pattern with depth of 50 nm. Wafers were then diced into 25 mm x 25 mm squares and then coated with titanium (5 nm) and gold (45 nm) using electron beam evaporation. Fabrication was performed at the SUNY Polytechnic Institute nanofabrication facility, in collaboration with Ciencia Inc (www.ciencia.com). A SEM image of sensor is shown in the Fig.1(c).

Fabricated GCSPR chips were tested using a custom-fabricated GCSPR/SPCE instrument at Ciencia Inc. and a resonance was observed at an angle of incidence $\theta = 10 \pm 2°$ for $\lambda = 633$ nm. Our model predicts a resonance peak at 12° as shown in Fig.2(a) , which is in good agreement with expermental observation.

6 APPLICATIONS

As discussed above, GCSPR sensors are used for biosensing and bioimaging applications. One such appliacation is diagnosis of disease. Thus, we performed an experiment to detect levels of blood serum antibodies raised against Lyme disease (*Borrelia burgdorferi*) infection in mice.

Detection of antibodies indicative of Lyme disease: GCSPR microarrays were fabricated as described above. and then spotted with protein antigens that are components of the Lyme disease causative agent, Borrelia burgdorferi. Blood serum from a mouse infected with this bacterium was then applied to the GCSPR chip, followed by labeling with fluorophore-labeled anti-moues IgG. The resulting SPCE image (Fig.3) shows that antibodies against three different variants of the DbpA antigen, as well as OspC and DbpB could be detected using SPCE. Antibodies against BmpA were not detected, which is likely due to low immune response to this antigen, not the SPCE assay itself.

Wavelength upconversion [14-16]: SPR sesnors can be used either in reflection mode or transmission mode depending on the application. For wavelength upconversion, a transmission mode sesnor is coupled with material doped with rare-earth metals like erbium. The sesnor parameters are adjusted to generate high transmission and less reflection at a desired wavelength. This can then be used for wavelength upconversion.

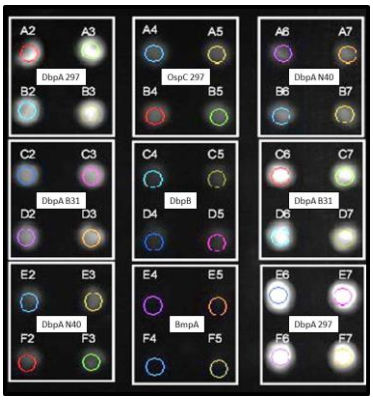

Figure 3: Detection of Lyme disease infection via SPCE. Blood serum from a mouse infected with Lyme disease was applied to a GCSPR chip pre-spotted with B. burgdorferi antigens (4 replicate spots per antigen). After secondary labeling with fluorophore-labeled anti-mouse IgG, the SPCE fluorescence image was collected, showing bright white spots where a strong antibody response occurred.

7 CONCLUSION

In this paper, we have discussed a COMSOL based computational model for designing thin film plasmonic grating structures. We performed parametric analysis to identify optimal parameters for sensor fabrication. The theoretical predictions are validated using experimental observations. Biosensing and wavelength upconversion applications are also discussed.

ACKNOWLEDGEMENTS

This work was supported by the U.S. National Science Foundation (NSF) under Grant No. IIP-1718177. The authors also acknowledge support from Dr. Yi-Pin Lin (Wadsworth Inst., NYS Department of Health) for providing Bb antigens and infected mouse serum. Authors also acknowledge support from Ciencia Inc. for GCSPR chip design and performance of SPCE measurements.

REFERENCES

1. Otto, A. Excitation of Nonradiative Surface Plasma Waves in Silver by Method of Frustrated Total Reflection. *Z Phys* **216**, 398-& (1968).
2. Kretschm.E & Raether, H. Radiative Decay of Non Radiative Surface Plasmons Excited by Light. *Z Naturforsch Pt A* **A 23**, 2135-& (1968).
3. Barnes, W.L., Dereux, A. & Ebbesen, T.W. Surface plasmon subwavelength optics. *Nature* **424**, 824-830 (2003).
4. Homola, J. Present and future of surface plasmon resonance biosensors. *Anal Bioanal Chem* **377**, 528-539 (2003).
5. Homola, J., Yee, S.S. & Gauglitz, G. Surface plasmon resonance sensors: review. *Sensor Actuat B-Chem* **54**, 3-15 (1999).
6. Mendoza, A., Torrisi, D.M., Sell, S., Cady, N.C. & Lawrence, D.A. Grating coupled SPR microarray analysis of proteins and cells in blood from mice with breast cancer. *Analyst* **141**, 704-712 (2016).
7. Sarid, D. & Challener, W.A. Modern introduction to surface plasmons : theory, Mathematica modeling, and applications. (Cambridge University Press, Cambridge ; New York; 2010).
8. Jager, K. et al. Simulations of sinusoidal nanotextures for coupling light into c-Si thin-film solar cells. *Opt Express* **24**, A569-A580 (2016).
9. Su, W. Design of high performance surface plasmon resonance biosensor using silver-based sinusoidal diffraction grating. *Optik* **131**, 104-109 (2017).
10. Etchegoin, P.G., Le Ru, E.C. & Meyer, M. An analytic model for the optical properties of gold. *J Chem Phys* **125** (2006).
11. Johnson, P.B. & Christy, R.W. Optical Constants of Noble Metals. *Phys Rev B* **6**, 4370-4379 (1972).
12. Sheng, P., Stepleman, R.S. & Sanda, P.N. Exact Eigenfunctions for Square-Wave Gratings - Application to Diffraction and Surface-Plasmon Calculations. *Phys Rev B* **26**, 2907-2916 (1982).
13. Jain, P.K., Huang, X., El-Sayed, I.H. & El-Sayad, M.A. Review of some interesting surface plasmon resonance-enhanced properties of noble metal nanoparticles and their applications to biosystems. *Plasmonics* **2**, 107-118 (2007).
14. Wang, F. & Liu, X.G. Upconversion multicolor fine-tuning: Visible to near-infrared emission from lanthanide-doped NaYF4 nanoparticles. *J Am Chem Soc* **130**, 5642-+ (2008).
15. Schietinger, S., Aichele, T., Wang, H.Q., Nann, T. & Benson, O. Plasmon-Enhanced Upconversion in Single NaYF4:Yb3+/Er3+ Codoped Nanocrystals. *Nano Lett* **10**, 134-138 (2010).
16. Greybush, N.J. et al. Plasmon-Enhanced Upconversion Luminescence in Single Nanophosphor-Nanorod Heterodimers Formed through Template-Assisted Self-Assembly. *Acs Nano* **8**, 9482-9491 (2014).